Optics Letters

Single-shot intense few-cycle pulse interaction with polycrystalline ZnSe

YINGJIE CHAI,[1] XIAOMING YU,[1] HE CHENG,[1] ANDREW CHEW,[1,2,3] ZENGHU CHANG,[1,2,3] MICHAEL BASS,[1,2] AND M. J. SOILEAU[1,2,4,*]

[1]CREOL, The College of Optics and Photonics, University of Central Florida, 4304 Scorpius Street, Orlando, Florida 32816, USA
[2]Department of Physics, University of Central Florida, 4111 Libra Drive, Orlando, Florida 32816, USA
[3]Institute for the Frontier of Attosecond Science and Technology, University of Central Florida, 4000 Central Florida Blvd., Orlando, Florida 32826, USA
[4]Department of Electric and Engineer and Computer Science, University of Central Florida, 4328 Scorpius Street, Orlando, Florida 32816, USA
*Corresponding author: mj@ucf.edu

Received 26 February 2020; revised 27 April 2020; accepted 7 May 2020; posted 7 May 2020 (Doc. ID 391361); published 4 June 2020

The interaction of high-intensity few-cycle laser pulses with solids opens a new area of fundamental light-material interaction research. The applied research extends from extreme nonlinearity in solids to the next-generation high laser light damage resistance optical design. In this Letter, 11 fs infrared, carrier-envelope-phase (CEP) stable, two-cycle laser pulses were applied to investigate the process of laser-material interaction on the ZnSe surface. A systematic study of a few-cycle pulse laser-induced damage threshold on ZnSe was performed for a single-pulse regime (1-on-1). Laser damage morphologies were carefully characterized. Our experiment demonstrated the very beginning of laser-induced structures on the ZnSe surface by using the shortest infrared few-cycle laser pulse currently available with a stable CEP.

https://doi.org/10.1364/OL.391361

A few-cycle pulse has revolutionized the field of intense-field physics with the advent of single attosecond pulses probing electron dynamics in atoms and molecules. Due to its immense promise of opening doors to new physics in relativistic regimes, there is a concerted effort to construct next-generation ultra-intense few-cycle pulse sources. Polycrystalline II-VI semiconductors (e.g., ZnSe, ZnS) are promising laser materials for the next generation of the high-power mid-infrared few-cycle laser source. Laser-induced damage on II-VI semiconductors has been studied since the early 1980s [1] and is commonly observed in the failure of an intense ultrashort laser system [2,3]. The long-cycle pulse experiment showed that the pulse can generate structures on the incident optic surface, providing opportunities to study laser-material interactions such as laser-induced carrier dynamics [4] and high-harmonic generation [5]. The nonlinear ionization process with >100 fs laser on a highly exited surface showed a unique phenomenon in ultrafast laser-material interaction dynamics. However, a long-cycle femtosecond laser pulse contains tens to hundreds of electromagnetic cycles [6]. From the long-cycle femtosecond damage remains, the initial step of laser-induced structures is still unknown. A deeper level of damage mechanism is still under investigation for a few-cycle laser, because the basic way to imply ripple formation was from the ablated remains. The morphologies of the highly excited surface rapidly evolved from the first few cycles to the last few cycles. In this Letter, experimental studies were designed to investigate the influence of ultrashort laser pulses on the damage behavior on the surface of ZnSe, an important material in the infrared region and for attosecond laser generation [7]. Near-infrared 11fs wide spectrum (1.2–2.2 μm) infrared few-cycle laser pulses were applied as an irradiation source [8]. By comparing the damage thresholds and morphologies for single-pulse laser damage, the beginning of laser-induced surface ripples on ZnSe was carefully investigated. Electron dynamics calculations were employed to explain the damage mechanism. Microstructure (cracks and ripples) evolution during laser irradiation on crystalline grain provides an explanation for the initial damage.

Chemical vapor deposited polycrystalline ZnSe was used in our experiment. No residual pores, secondary phases, or optically inhomogeneity were observed, and the number of point and line defects and dislocations were at a minimum level in the grains [9]. Grain boundaries, at the atomic scale, can influence the incident electronic-field (E-field) [10]. Grain boundaries were exposed clearly by chemical etching [11] of a NaOH solution [see Figs. 1(A1) and 1(A2)]. The chemical vapor deposited ZnSe has a polycrystalline grain size of lognormal distribution with an average grain size of ∼30 μm [12], as shown in Fig. 1(B).

In our Letter, the laser-induced damage threshold (LIDT) measurements were implemented in accordance with ISO 21254 for 1-on-1 irradiation and shown in Fig. 2(A). A 3 mJ, two-cycle, 1 kHz and carrier-envelope-phase stable infrared light source were used to perform the few-cycle laser damage experiment, with detail introduced in Ref. [8]. A practical and compact laser-induced damage test platform was employed right after the OPCPA system; more details of the 1.7 μm few-cycle laser source are shown in Fig. 2(A). The ZnSe sample was fixed on a computer-controlled $X-Y-Z$ stage. The beam was focused by a parabola to prevent unnecessary pulse width

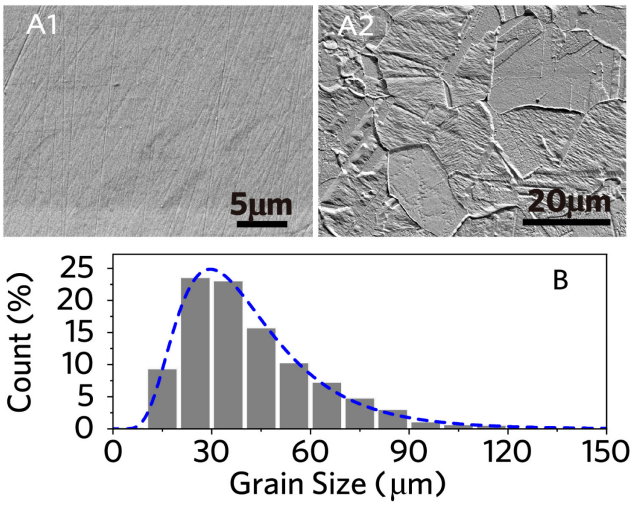

Fig. 1. ZnSe Surface morphologies (A) before and (B) after NaOH etching. The grain boundaries were exposed with an average size of 30 μm (lognormal distribution).

elongation. The damage spot size was extracted by a commercial beam profiling camera, and the $1/e^2$ Gaussian beam diameter is 230 μm. The few-cycle laser has a central wavelength at 1.7 μm [wide spectrum covers 1.2–2.2 μm, as shown in Fig. 2(B)] with a pulse width of 11 fs. A 1-on-1 LIDT of ZnSe was 89 mJ/cm^2, as shown in Fig. 2(C). The damaged spot size in diameter was much smaller than the $1/e^2$ diameter of the incident laser

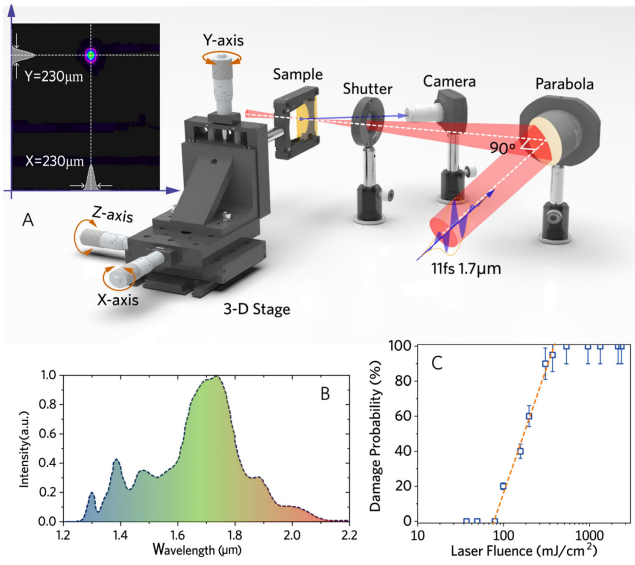

Fig. 2. Terminal position of a few-cycle laser-induced damage test platform. The three-dimensional sample holder was controlled by a stepper motorized actuator. A mechanical shutter was used for pulse number control. (A) A long-distance camera was employed to online monitoring the damage morphologies. Focused by a parabola, the laser spot size was extracted from a commercial beam profiler. (B) Output spectrum of the few-cycle laser source. (C) Laser-induced damage probabilities with different intensity. The red curve indicates that the linear fitting of damage probability ranged from 0% to 100%. We considered a zero-laser-induced damage threshold as the highest laser fluence without surface damage which happened according to ISO 21254.

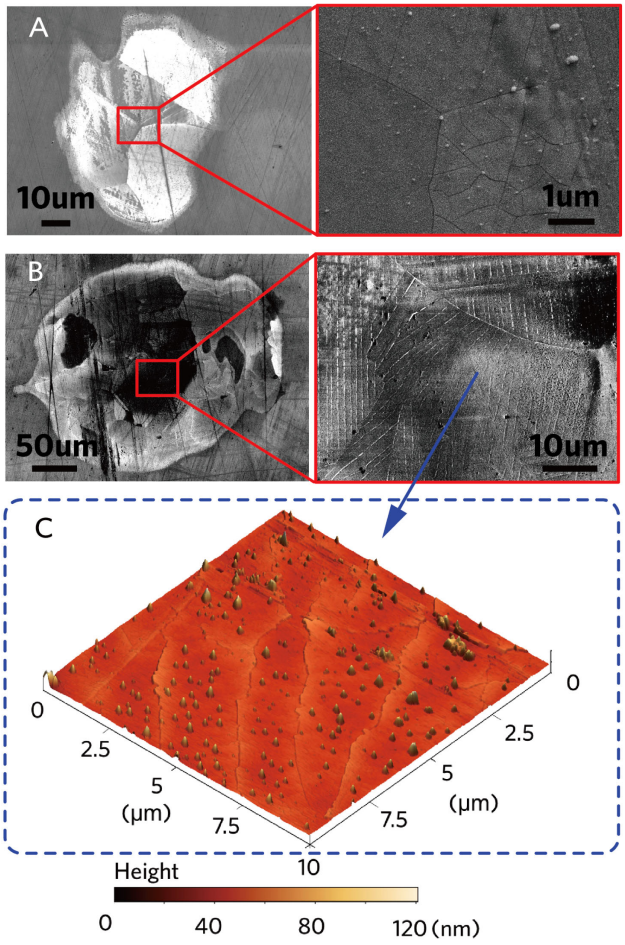

Fig. 3. (A) Near threshold damage site with 157 and (B) 500 mJ/cm^2 irradiation. High-density cracks showed in the central area of the Gaussian spot from high-resolution SEM characterization. (C) AFM image from the shallow cracks zone. The crack width is 50–80 nm, and the depth is 5–10 nm as extracted from AFM software.

beam, which means multi-photon ionization occurred in the damaged area, as shown in Fig. 3. The higher laser incident fluence-induced larger damage site, as compared in Figs. 3(A) and 3(B). Laser ablation morphologies showed no melting in the first pulse, and mechanical cracks associated with microcrystal grain boundaries were observed from AFM image; see Fig. 3(C). The crack period varied from 1.0–2.5 μm as extracted from high-resolution SEM image. Initial laser-induced structures were generated with seemly random orientations. However, when we look back to the etched ZnSe surface in Fig. 1, the randomly distributed orientations seem reasonable. Here, for one few-cycle shot, we did not observe the surface ripple patterns, which commonly exist in long-cycle laser interaction with materials [1]. The ZnSe grain boundary plays an important role in the very beginning of ablation structures. Perturbation to the e-field will occur with a certain shape of grain boundary-induced cracks. According to the quasi-static model proposed by Temple and Soileau in the literature [1]: time retardation surface waves are overlapped on subsequent pulse cycles and cause laser-induced damage orthogonal to the impressed field, which are spaced at approximately a wavelength. The resultant structures were resonating with subsequent cycles, reinforcing

and growing the observed ripple patterns. However, unlike the long cycle, the few-cycle pulse has an extremely high e-field intensity ratio between cycles. When the sample is irradiated by near-threshold intensity, ionization energy was concentrated in the central (peak) cycle, and the neighborhood cycle intensity decreased by several orders of magnitude. In this condition, interference between the induced surface wave and the next cycle e-field does not reach the LIDT, and eventually no ripples were generated. Slight surface modification must happen at the expected spacing of the first ripple, but is below detectability for single pulses. Few-cycle laser-induced ripples showed with high-intensity multi-pulse accumulation. The N-on-1 LIDT results/morphologies were experimentally demonstrated in Ref. [13], and their complex damage mechanisms will be investigated and performed in future research.

During the laser-material interaction, the few-cycle laser pulses can give rise to sub-cycle oscillations of electron density in solids. The ultrashort laser-induced ionization breakdown was defined as the threshold when a certain fraction of critical electron density was generated within the incident laser pulse. In few-cycle ionization dynamics, the critical electron density is defined as [14]

$$\rho_c = \frac{m^* \omega^2}{4\pi e^2}, \tag{1}$$

where e is the electron charge, m^* is the effective mass, and ω is the plasma frequency. The ρ_c for ZnSe is in the range $3.92 \times 10^{19} \sim 13.18 \times 10^{19}/\mathrm{cm}^3$ for our wavelength range of 1.2–2.2 μm. The central spectral wavelength of 1.7 μm has a critical density of $\rho_{c0} = 6.56 \times 10^{19}/\mathrm{cm}^3$. Here we presume that the electron effective recombination time can be ignored in our experiment because the 11 fs few-cycle laser pulse is far

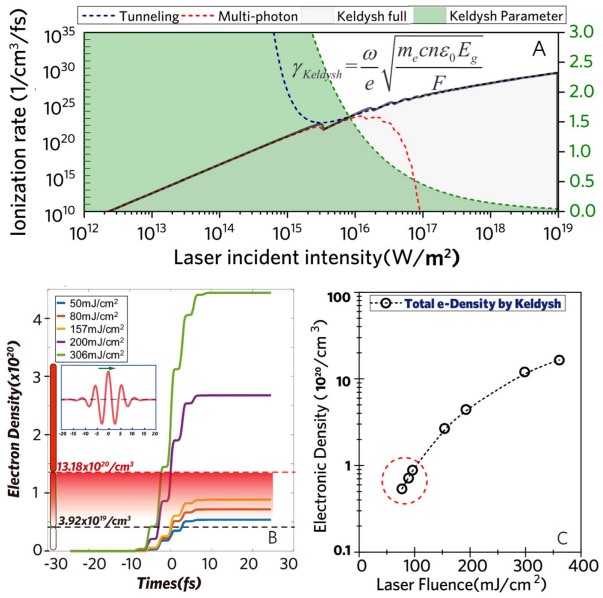

Fig. 4. (A) Intermediate value Keldysh parameter γ was used to distinguish the $W_{\mathrm{MPI}}(F)$ and $W_{\mathrm{Tunnel}}(F)$ ionization dominant with high-intensity laser irradiation. (B) Electron density calculated by a Keldysh simulation with a laser fluence of $50 \sim 306\ \mathrm{mJ/cm}^2$. The gradient red zone demonstrates the critical density of the incident frequency range. (C) Final electron density extracted from the Keldysh calculation. The datapoint in the red dashed circle demonstrates the electron density near ρ_{c0}.

shorter than the normal decay time, and the electron decoherence effects are negligible on this time scale. Laser-induced avalanching was not considered in the 1-on-1 laser damage case. Multiphoton and tunneling ionizations were introduced in the calculation according to the Keldysh theory.

With a central wavelength of 1.7 μm, a temporal field of the incident few-cycle laser pulse can be found, and the time evolution of the ionized electron density can be calculated. An electron density calculation based on the Keldysh theory is a good tool to analyze the electron density evolution. The rate equation [Eqs. (2)–(5)] commonly used to predict the evolution of ionization electron density N is given by Eq. (2), where $W_{\mathrm{MPI}}(F)$ represents the multiphoton ionization rate, and $W_{\mathrm{Tunnel}}(F)$ represents the tunneling ionization rate. The Keldysh parameter γ was used as an intermediate variable to distinguish the multiphoton dominant ionization, tunneling dominant ionization, or a mixture of both [4,14,15]. The key value of γ is 1.5. As calculated and shown Fig. 4(A), when $\gamma \ll 1.5$, photoionization is tunneling ionization dominant; when $\gamma \gg 1.5$, photoionization is a multiphoton process; the intermediate regime where both tunneling and multiphoton ionization contribute occurs when the parameter is close to 1.5:

$$\frac{dN(t)}{dt} = W_{\mathrm{MPI}}(F) + W_{\mathrm{Tumnel}}(F), \tag{2}$$

$$W_{\mathrm{MPI}}(F) = \frac{2\omega}{9\pi}\left(\frac{m_e\omega}{\hbar}\right)^{1.5}\phi\left[\left(2\left(\frac{E_g^*}{\hbar\omega}+1\right)-\frac{2E_g^*}{\hbar\omega}\right)^{0.5}\right] \times \exp\left[2\left(\frac{E_g^*}{\hbar\omega}+1\right)\left(1-\frac{e^2F^2}{4m_e\omega^2E_g}\right)\right] \times \left(\frac{e^2F^2}{4m_e\omega^2E_g}\right)\left(\frac{e^2F^2}{16m_e\omega^2E_g}\right)^{\left(E_g^*+1\right)/\hbar\omega^2}, \tag{3}$$

$$W_{\mathrm{Tunnel}}(F) = \frac{2}{9\pi^2}\frac{E_g}{\hbar}\left(\frac{m_eE_g}{\hbar^2}\right)^{1.5}\left(\frac{e\hbar F}{m_e^{0.5}E_g^{1.5}}\right)^{2.5} \times \exp\left[-\frac{\pi}{2}\frac{m_e^{0.5}Eg^{1.5}}{e\hbar F}\left(1-\frac{1}{8}\frac{m_e\omega^2E_g}{e^{2F^2}}\right)\right], \tag{4}$$

$$E_g^* = E_g + \frac{e^2F^2}{4m_e\omega^2}; \quad \phi(x) = e^{-x^2}\int_0^x e^{-t^2}dt. \tag{5}$$

Here ZnSe has a bandgap of $\mathbf{E_g} = 2.71$ eV [4,16], $\mathbf{e}$ is the electron charge, $\mathbf{m_e}$ is the material electron effective mass, $\boldsymbol{\omega}$ is the radial frequency of the incident light, $\mathbf{F}$ represents the electric field strength, $\mathbf{E_g^*}$ is the effective ionization potential, and $\boldsymbol{\phi}$ is Dawson's integral. The electron density $N(t)$ was determined by MATLAB integrals [2]. In Fig. 4, ionization electron density increased in a stair-step shape because the ionization rate is sensitive to the instantaneous E-field. As shown in Fig. 4(B), with irradiation of 32 mJ/cm^2, the electron density is lower than ρ_{c0}. The near-threshold 89 mJ/cm^2 pulse had a peak intensity near 10 TW/cm^2, which induced the laser-material interaction in the photoionization scenario. Electron density reaches critical density near $10^{20}/\mathrm{cm}^3$ as extracted at the end

of the pulse. The total electron densities were higher than ρ_{c0}. Figure 4(C) extracted the final electron density in pulse duration time with different laser intensity incidence. The electron density increased rapidly, as laser intensity increased and catastrophic single-shot ionization happened once the electron density exceeds the critical density.

The bandgap, for a perfect single-crystal ZnSe, is completely clear of states. However, grain boundaries, which were used to distinguish structure between single- and polycrystalline materials, are common in ZnSe samples. ZnSe grain boundaries have a lower bandgap than the crystal bulk [17]. As a result, the material near the grain boundaries is more easily damaged photoionization. The polycrystalline nature of the sample makes the grain boundary the most vulnerable part of the sample for the irradiated high-intensity few-cycle laser.

In conclusion, a few-cycle laser-induced damage study of ZnSe with single-pulse damage behavior was studied. We found that the laser-induced damage threshold is ~89 mJ/cm^2. Laser-induced damage cracks were originated from the polycrystalline grain boundaries. High-resolution images revealed that the cracks were not well oriented after the first pulse. According to the quasi-static model [1], even the perturbation to the e-field occurred with a certain shape of grain boundary-induced cracks, and there is no stable polarization charge formed on the dielectric discontinuities within the pulse duration time. In other words, a one-shot few-cycle pulse is too short to generate ripples in our experiment. A wide spectrum few-cycle laser source-induced ~1.5 μm ripples showing that the period might have no clear relation with the incident light wavelength. Our experiment showed that after a single pulse, the ripple structures are not uniformly oriented because of the polycrystalline nature of the ZnSe material. An electron density simulation based on the Keldysh theory indicates the few-cycle laser damage occurs where the laser intensity is such that it generates a certain fraction of critical electron density (ρ_{c0}) within the pulse duration. A multi-shot laser damage experiment will be conducted in the future work, and we plan to extend this study to different infrared materials for increasing our understanding of laser-induced interactions between ultrashort few-cycle laser light and more complex optics.

Funding. Preeminent Postdoctoral Program Award from the College of Graduate Studies at the University of Central Florida (P3 award); Florida Space Institute; The Florida High Tech Corridor; Materials Characterization Facility, Advanced Materials Processing and Analysis Center, University of Central Florida.

Acknowledgment. The authors thank Dr. Romain Gaume and Dr. Xuan Chen for their assistance with ZnSe characterization. The authors thank Dr. Laurene Tetard and Dr. Yi Ding for their assistance with AFM characterization.

Disclosures. The authors declare no conflicts of interest.

REFERENCES

1. P. A. Temple and M. J. Soileau, IEEE J. Quantum Electron. **17**, 2067 (1981).
2. S. Z. Xu, T. Q. Jia, H. Y. Sun, C. B. Li, X. Li, D. H. Feng, J. R. Qiu, and Z. Z. Xu, Opt. Commun. **259**, 274 (2006).
3. Y. Y. Dong and P. Molian, Appl. Phys. Lett. **84**, 10 (2004).
4. V. Gruzdev and O. Sergaeva, Phys. Rev. B **98**, 115202 (2018).
5. T. Q. Jia, H. X. Chen, M. Huang, F. L. Zhao, J. R. Qiu, R. X. Li, Z. Z. Xu, X. K. He, J. Zhang, and H. Kuroda, Phys. Rev. B **72**, 125429 (2005).
6. E. M. Hsu, T. H. R. Crawford, H. F. Tiedje, and H. K. Haugen, Appl. Phys. Lett. **91**, 111102 (2007).
7. X. M. Ren, L. H. Mach, Y. C. Yin, Y. Wang, and Z. H. Chang, Opt. Lett. **43**, 3381 (2018).
8. Y. C. Yin, J. Li, X. M. Ren, K. Zhao, Y. Wu, E. Cunningham, and Z. H. Chang, Opt. Lett. **41**, 1142 (2016).
9. A. Ikesue and Y. L. Aung, Nat. Photonics **2**, 721 (2008).
10. G. J. Russell, M. J. Robertson, B. Vincent, and J. Woods, J. Mater. Sci. **15**, 939 (1980).
11. H. Oczkowsi and Z. Poplawski, J. Cryst. Growth **23**, 154 (1974).
12. M. F. Vaz and M. A. Fortes, Scripta Metall. Mater. **22**, 35 (1988).
13. Y. J. Chai, H. Cheng, X. Yu, A. Chew, X. M. Ren, Z. H. Chang, and M. J. Soileau, Proc. SPIE **10805**, 108050O (2016).
14. P. A. Zhokhov and A. M. Zheltikov, Sci. Rep. **8**, 1824 (2018).
15. P. A. Zhokhov and A. M. Zheltikov, Phys. Rev. Lett. **113**, 133903 (2014).
16. S. Adachi and T. Taguchi, Phys. Rev. B **43**, 9569 (1991).
17. F. Frost, B. Ziberi, A. Schindler, and B. Rauschenbach, Appl. Phys. A **91**, 551 (2008).